Probing Thermal Flux in Twinned Ge Nanowires through Raman Spectroscopy

Dipanwita Majumdar[1], Subhajit Biswas[2], Tandra Ghoshal[3], Justin D. Holmes [2,4], Achintya Singha[1*]

[1]Department of Physics, Bose Institute, 93/1, Acharya Prafulla Chandra Road, Kolkata 700009, India

[2]Materials Chemistry & Analysis Group, Department of Chemistry and the Tyndall National Institute, University College Cork, Cork, Ireland

[3]Materials Research Group, Department of Chemistry and the Tyndall National Institute, University College Cork, Cork, Ireland

[4]AMBER@CRANN, Trinity College Dublin, Dublin 2, Ireland

*Author to whom correspondence should be addressed. Electronic mail: achintya@jcbose.ac.in Phone: + 91 33 23031177, Fax: + 91 33 23506790

ABSTRACT

We report a noninvasive optical technique based on micro Raman spectroscopy to study the temperature dependent phonon behavior of normal (non-defective) and twinned germanium nanowires (Ge-NWs). We have studied thermo-physical properties of Ge-NWs from Raman spectra, measured by varying excitation laser power at ambient condition. We have derived the laser induced temperature rise during Raman measurements by analyzing the Raman peak position for both the NWs and for a comparative study we have performed the same for bulk Ge. The frequency of the Ge-Ge phonon mode softens for all the samples with the increase in temperature and the first order temperature coefficient (χ_T) for defected NW is found to be higher than normal NW and bulk. We have demonstrated that apart from the size, the lamellar twinning and polytype phase drastically affect the heat transport properties of NW.

KEYWORDS: Germanium nanowire, polytype phase, Raman spectroscopy, laser induced heating, Thermal properties

INTRODUCTION

Germanium (Ge) nanowires (NWs) have a wide range of potential applications in optoelectronics, photovoltaics and biological sensing[1-10] due to low band gap energy (0.67 eV at room temperature) and high hole mobility (2000− 4000 $cm^2 V^{-1} s^{-1}$).[11] Though single crystalline NWs are high on demand for device implementation, crystal structure engineering via defects in semiconductor NWs is gaining interest in the past few years due to interesting mechanical, thermoelectrical and electronic properties of defect-engineered nanostructures. Presence of crystal defect in the form of twins alter their band structure and hence mobility of electron and holes.[12-14] Also, the defects can change the phonon frequencies, unit cell volume and strain, which result in modification of thermal conductivity of the material. [15-19] Moreover, the presence of defects could also modify the phonon dispersion relation, thus the change of phonon transport, which in turn affects the thermal conductivity of the NW.[19,20] Therefore, the knowledge of thermal properties of twinned/defected NWs is crucial for their performance in future applications such as nanoscale electronics,[21-22] sensors,[24,25] photonic device,[26,27] solar cell and thermoelectric devices.[28,29] Temperature dependent phonon behavior of defect free Ge NWs has been investigated recently in the temperature range above 300 K.[30] However, to the best of our knowledge, no systematic experimental results have been reported on the thermal conductivities of Ge NW with coherent twinning and polytype. A contactless optical method is crucial for the study of thermal property in small length scale.[31]

Raman spectroscopy has been used successfully as a simple and convenient method for studying thermal properties of different materials.[32-43] The laser beam in Raman spectrometer plays two different roles. First, it is a source of photon, which is inelastically scattered by the matter, providing Raman effect; and second, it serves as a heat source that can significantly

increase the local temperature of a material with the absorption of incident photons. The increase in local temperature depends on the thermal conductivity of the materials. Therefore, laser power dependent Raman study enables to investigate the thermal properties of materials.[32-43]

In this article, using Raman spectroscopy, we explore the impact of twin defects on the thermal properties of Ge NWs. The analysis of Raman spectra acquired at different laser powers from normal and twinned NWs has been carried out in detail. Based on the parameters obtained from the analysis of Raman spectra, we have estimated local temperature rise in the NWs during the measurements and compared the results with bulk Ge. We have estimated first order temperature coefficient of all the three systems and compared the thermal conductivity between the two types of NWs. We believe that our work will establish Raman spectroscopy as a simple and nondestructive tool to understand the thermal properties of NWs with lamellar twinning and local polytypes.

EXPERIMENTAL SECTION

Block Co-polymer patterned magnetite nanodot catalyst synthesis: Ge nanowires were seeded from magnetite iron oxide catalysts patterned through block co-polymer (BCP) lithography.[44] For BCP nanodot synthesis the polystyrene-b-poly(ethylene oxide) (PS-b-PEO) diblock copolymer was purchased from Polymer Source and used without further purification (number-average molecular weight, M_n, PS = 42 kg mol^{-1}, M_n, PEO = 11.5 kg mol^{-1}, M_w/M_n = 1.07, M_w: weight-average molecular weight). Substrates were cleaned by ultrasonication in acetone and toluene for 30 min in each solvent and dried under a nitrogen stream. PS-b-PEO was dissolved in toluene to yield a 0.9 wt% polymer solution at room temperature. The PS-b-PEO thin film was formed by spin coating the polymer solution (3000 rpm for 30 s). The film was exposed to

toluene/water (50:50 v/v) mixed vapor placed at the bottom of a closed vessel kept at 50 °C for 1h under a static vacuum. The film was immersed in ethanol at 40 °C for 15 h to obtain the activated thin film. Different concentrations of iron (III) nitrate nonahydrate ($Fe(NO_3)_3,9H_2O$) were dissolved in ethanol and spin-coated onto the activated film. UV/Ozone treatment was used to oxidize the precursor and remove the polymer.

Ge Nanowire Synthesis: Continuous-flow reactions for nanowire growth were carried out in a toluene medium using a liquid-injection chemical vapor deposition (LICVD) technique. BCP – patterned Fe_3O_4 nanodots on a Si (001) substrate were loaded into a stainless steel microreactor cell, connected to metal tubing. The reaction cell and connections were dried for 24 h at 180 ºC under vacuum. Solutions of diphenylgermane (DPG), the Ge precursor, in anhydrous toluene were prepared in an N_2 glove box with a typical concentration of 4 μmole ml^{-1}. A DPG solution was loaded into a Hamilton sample-lock syringe inside a nitrogen-filled glovebox. The precursor solution was then injected into the stainless steel reaction cell using a high-pressure syringe pump at a rate of 0.04 ml min^{-1}. A H_2/Ar flow rate of 0.5 ml min^{-1} was maintained during the entire growth period. The reaction cell was allowed to cool to room temperature and disassembled to access the growth substrate. Nanowires were washed with dry toluene and dried under N_2 flow for further characterization.

Characterization

The 1D Ge nanostructures were analyzed using a FEI quanta 650 scanning electron microscope (SEM) and a Jeol 2100 transmission electron microscope (TEM) operated at 200 kV equipped with an EDX detector. Raman spectra were collected using a Lab RAM HR (Jobin Yvon) spectrometer equipped with 1800 gr/mm grating and Peltier cold CCD detector. An air-cooled

argon-ion laser (Ar^+) of wavelength 488 nm was used as excitation light source and a 100X objective with numerical aperture (NA) of 0.9 was used to focus the laser on the sample and to collect the scattered light from the sample. To measure the laser power dependent Raman spectra, the NWs were placed on a silicon nitride (SiN) TEM grid with FIB patterned hollow trench. Each trench was marked with a certain number to correlate the structure of the NW with Raman spectroscopy measurements. NWs were dropcast on this patterned TEM grids and checked thoroughly under TEM observation. Normal and twinned NWs were marked with respect to the SiN trench numbering scheme and the laser beam from the Raman spectrometer was tightly focused on the particular NW. Due to poor thermal contact of the NW with the grid, the intense laser beam in micro Raman spectrometer can lead to a significant heating of the nanowire. For each laser power, the Raman data were taken after 5 minutes of laser irradiation to reach equilibrium state of heating by the laser.

RESULTS AND DISCUSSION

Ge NWs with a mean diameter of 20.8 nm are grown from BCP patterned magnetite catalysts with the radial dimension of ~ 21 nm. The lengths of the Ge NWs synthesized were between 2 to 5 microns. These particular magnetite nanodot catalysts are suitable for growth of large numbers of <111> oriented Ge NWs with transverse twin boundaries; i.e. lateral growth of twin planes perpendicular to the nanowire growth axis (15-20 %, based on studying 250 nanowires per sample).[44] Induction of the heterogeneously distributed multiple layer {111} twins, directed perpendicular to the NW growth axis, is due to the particular curvature of the catalyst-substrate and catalyst-NW interface and adherence of the BCP patterned nanodots with substrate.[45] The detailed structural nature of the densely twinned NWs was analyzed through high-resolution

transmission electron microscope (HRTEM). The HRTEM images of normal (defect free) and twinned NWs are shown in Figure 1(a) and (b), respectively. The fast Fourier transform pattern (FFT) of normal NW shows the structure is pure diamond cubic Ge phase (3C-Ge) with <111> growth orientation. HRTEM observations from defected NW confirm the occurrence of {111} transverse twin boundaries perpendicular to the nanowire <111> growth direction. A 60° rotation of crystal orientation on the both sides of the twin planes with the growth axis represents a mirror reflection of a 3C stacking order of the {111} planes without any bond-breakage at the interface. The HRTEM image shown in Figure 1(b) is viewed along the <110> zone axis. Periodic modulations of altering (-1-11) and (-1-1-1) 3C cubic lateral facets were observed when viewed along the <110> zone axis. VLS growth of Si or Ge NWs does not permit the formation of periodic twins in <111> directed nanowires because of the small wetting angle variation at the triple-phase interface.[46] Whereas for Fe_3O_4 seeded Ge nanowire growth, heteroepitaxy and strain at the catalyst-NW interface is more liable for the triggering of twin boundary nucleation. Periodic twinned planes can generate polytype superstructures, where stacking faults in the *abc* stacking sequence along the <111> direction can produce local hexagonal ordering in a cubic crystal, for example, *aba*, leading to polytypes with distinctly unique properties. In the densely faulted regions of a NW, *i.e.* in NWs with a high twin density, successive {111} stacking faults result in a change in the stacking sequence from 3C to other polymorphs. In the analyzed NW, cubic 3C stacking in tetrahedral coordination in the <111> direction changed locally to 4H polytypes in the regions with dense twin formation (Figure 1(b)).

For further confirmation of crystal structure, Raman scattering measurements were performed on both normal and twinned NWs, and the measured spectra are presented in Figure 1(c) (normal NW) and (d) (polytype NW). The peak due to triply degenerated E_{2g} vibration (Ge-

Ge mode) appears at 299.5 and 298 cm^{-1} in normal and polytype NWs, respectively. The same mode in bulk Ge appears at 300 cm^{-1} as shown in the inset of Figure 1(c). The possible origins of the frequency red shift are laser induced heating, confinement effect and strain. The measurements were carried out at very low laser power, which excludes the laser induced heating effect. It is known that 3C-Ge exhibits a slightly larger lattice parameter than 4H-Ge.[12] This mismatch can create an intrinsic compressive strain in the 3C region. Therefore, we should expect a blue shift of the Ge-Ge mode in polytype NW, which is opposite to our experimental observation. The NWs are in a floating state on the SiN patterned substrate without any attachment at the end and no uniaxial, or biaxial strain was applied intentionally to the NWs. But, some additional strain may be developed due to the hanging of the NW on the hollow trench of SiN, which may cause some frequency change. The Ge-Ge mode also shifts towards lower frequency due to the confinement of phonon in the nanostructure.[40] In normal NW, the confinement effect is weak (diameter of NW~40 nm) but in defected NW, the presence of 4H-Ge phase divides the NW in small segments, where the confinement effect is probably higher. The space resolved Raman study could provide the role of strain in the NW.[47] In addition to the mode at 298 cm^{-1}, the presence of another peak at 284 cm^{-1} in twinned NW indicates the existence of polytype phase, which is also confirmed by TEM analysis of corresponding Ge NWs (Figure 1(b)) and is consistent with the earlier reports. [13,45,48] The hexagonal 4H-Ge region can form a region up to few nanometers with altered band structure in a 3C-Ge NW host lattice.[12,13]

To measure the laser power dependent Raman spectra, the laser power was varied from 0.2 mW to 30 mW, and the corresponding Raman spectra of the normal and polytype NWs were recorded, which is displayed in Figure 2(b) and (c), respectively. For reference, the same measurement has been performed on bulk Ge, which is shown in Figure 2(a). To get the peak

position and full width at half maxima (FWHM), the spectra are fitted with Lorentzian function. Figure 3(a), (b) and (c) show the variation of peak positions as a function of laser power for bulk Ge, normal NW and polytype NW, respectively. The peak positions decrease as we increase the laser power, which indicates that the local temperature of the samples increases due to laser irradiation.[40,49,50] The factors that influence the temperature dependence of Raman shifts and line widths are anharmonic phonon-phonon interaction and thermal expansion.[40,50] The frequency shift due to phonon-phonon coupling is represented by (considering three-phonon coupling) [40,50]

$$\Delta\omega_1(T) = A[1 + \frac{2}{e^{\hbar\omega_0/2k_BT} - 1}] \qquad (1)$$

where ω_0 is the Raman frequency at 0 K and A is anharmonic constant.

The contribution of thermal expansion to the Raman frequency shift can be expressed as [40,50]

$$\Delta\omega_2(T) = \omega_0[\exp(-3\gamma\beta T) - 1] \qquad (2)$$

where γ is Gruneisen parameter and β is the thermal expansion coefficient of Germanium.

The FWHM can be expressed in terms of Bose-Einstein function as the energy of band transition thresholds decreases in proportion to the Bose-Einstein factors,[40, 49-53]

$$\Gamma(T) = \Gamma_0[1 + \frac{2}{e^{\hbar\omega_0/2k_BT} - 1}] \qquad (3)$$

where Γ_0 is the FWHM at 0 K. From the intensity ratio between anti-Stokes and Stokes lines, the sample temperature can be calculated but anti-Stokes peak cannot be recorded in our setup. Alternatively, the peak position or peak width could be used as a temperature indicator. The temperature dependent Raman shift is independent of factors such as resonant Raman, absorption, fluctuation in pulse intensity, etc.[32] So, the uncertainties in estimating the temperature from the peak positions are lower than those from the peak width. We have

estimated the laser induced temperature using the values of the parameters used in Ref. 50 and the experimentally obtained laser power dependent phonon frequency shift, combining equation (1) and (2). The calculated temperature as a function of laser power for bulk Ge, normal NW and polytype NW are displayed in Figure 3(d), (e) and (f), respectively. In both the normal and defective NWs, the maximum temperature reaches around 700 K at laser power below 30 mW whereas in bulk Ge the temperature reaches around 500 K at 30 mW laser power. The local temperature rise depends on the heat transport properties of the materials. Local temperature increase will be lower for a material with higher thermal conductivity. A faster increase in temperature is observed in NWs compared to bulk Ge due to the combination of several factors. Firstly, due to large surface-to-volume ratio, boundary scattering of electrons and phonons is significant in NWs, which reduce the thermal conductivity and allow the nanowire to heat up easily.[54] Secondly, the heat transport by low frequency phonon, which is substantial in bulk systems, cannot survive in the NWs because the mean free path of the phonons is longer than the size of the NWs.[54] Finally, in the low dimensional systems the confinement of phonon modifies the phonon transport properties.[55] The role of twin boundaries and 4H polytype arrangement in affecting the thermal conductivity of nanostructure is discussed in the section below.

Figure 4(a), (b) and (c) show the position of the Ge-Ge mode as a function of temperature due to laser induced heating for bulk Ge, normal NW and polytype NW. The Raman frequencies decrease monotonically with the temperature. To analyze the red shift in the Ge-Ge mode with temperature we used a linear change in energy as [41,42]

$$\omega(T) = \omega_0 + \chi_T T \qquad (4)$$

where ω_0 is the phonon frequency at zero temperature and χ_T is the first order temperature coefficient. By fitting the phonon downshift using equation (4), the obtained χ_T values for bulk

Ge and normal NW are -0.02088 cm^{-1}/K and -0.02089 cm^{-1}/K, respectively. The χ_T for both bulk Ge and normal NW are in good agreement with reported value (-0.02000 cm^{-1}/K),[50] indicating that the method used to determine the local temperature is reasonable although the accurate temperature determination using this method is non-trivial. The first order temperature coefficient of twinned/polytype NW is -0.02239 cm^{-1}/K, which is higher than the bulk and normal NW. The reason could be the modification of phonon dispersion curve and electron–phonon coupling due to the presence of polytype phase. Further, study is needed to clarify this effect. The presence of twin boundaries, the increased number of interfaces will lead to an enhanced interface scattering, which is responsible for the reduction in thermal conductivity with respect to the normal NW. To get a quantitative comparison of thermal conductivity between normal and defective NWs, we have estimated slope ($d\omega/dP$, where P is the laser power) by fitting the data presented in the left panel of Figure 3. The solid lines are the linear fit to the experimental data. The values of slopes for normal and polytype NWs are -0.2715 cm^{-1}/mW and -0.3232 cm^{-1}/mW, respectively. In terms of $d\omega/dP$ the thermal conductivity (k) can be written as[56]

$$k = \chi_T \left(\frac{1}{2\pi d}\right)\left(\frac{d\omega}{dP}\right)^{-1} \qquad (5)$$

We consider absorption power of both the NWs is same as they are equal in size, and experimental conditions were identical. We have found that the thermal conductivity of the polytype NW is approximately 10% lower than the normal NW. The low thermal conductivity of nanofaceted twinned/polytype NWs compared to their smooth faceted counterpart could make them ideal candidates for thermoelectric applications.[55]

CONCLUSIONS

In conclusion, we successfully introduced laser induced heating during Raman measurements to study temperature dependent phonon behavior of normal and polytype Ge NWs. We have estimated the first order temperature coefficient of phonon shifts in both normal and defected NWs and compared their thermal conductivity. Demonstration of altered phonon dynamics in twinned/polytype nanowires for a reduced thermal conductivity makes these innovative nanostructures suitable for thermoelectric devices. Use of noncontact and uncomplicated spectroscopic tool to study the local heating behavior in nanoscale is useful for a simple and reliable investigation of the thermal properties of innovative nanostructures.

Acknowledgements

We acknowledge financial support from Science Foundation Ireland (SFI) International Strategic Co-operation Award (ISCA) India-Ireland program.

REFERENCE

1 Burchhart, T.; Zeiner, C.; Lugstein, A.; Henkel C.; Bertagnolli, E. Tuning the Electrical Performance of Ge Nanowire MOSFETs by Focused Ion Beam Implantation. *Nanotechnology* **2011**, *22*, 035201-(4 pp).

2 Garnett E.; Yang, P. D. Light Trapping in Silicon Nanowire Solar Cells. *Nano Lett.* **2010**, 10, 1082-1087.

3 He, R. R.; Gao, D.; Fan, R.; Hochbaum, A. I.; Carraro, C.; Maboudian R.; Yang, P. D. Si Nanowire Bridges in Microtrenches: Integration of Growth into Device Fabrication. *Adv. Mater.* **2005**, 17, 2098-2102.

4 Leonard, F.; Talin, A. A.; Swartzentruber B. S.; Picraux, S. T. Diameter-Dependent Electronic Transport Properties of Au-Catalyst/Ge-Nanowire Schottky Diodes. *Phys. Rev. Lett.* **2009**, *102*, 106805-4.

5 Liu, Y.-C. C.; Rieben, N.; Iversen, L.; Sorensen, B. S.; Park, J.; Nygard J.; Martinez K. L. Specific and Reversible Immobilization of Histidine-Tagged Proteins on Functionalized Silicon Nanowires. *Nanotechnology* **2010**, 21, 245105-(7pp).

6 Seo, M. H.; Park, M.; Lee, K. T.; Kim, K.; Kim, J.; Cho, High Performance Ge Nanowire Anode Sheathed with Carbon for Lithium Rechargeable Batteries. *J. Energy Environ. Sci.* **2011**, 4, 425-428.

7 Biswas, S.; Singha, A.; Morris M. A.; Holmes, J. D. Inherent Control of Growth, Morphology, and Defect Formation in Germanium Nanowires. *Nano Lett.* **2012**, 12, 5654-5654.

8 Wu, X. Y.; Kulkarni, J. S.; Collins, G.; Petkov, N.; Almecija, D.; Boland, J. J.; Erts, D.; Holmes, J. D. Synthesis and Electrical and Mechanical Properties of Silicon and Germanium Nanowires. *Chem. Mater.* **2008**, *20*, 5954-5967.

9 Xiang, J.; Lu, W.; Hu, Y. J.; Wu, Y.; Yan, H.; Lieber, C. M. Ge/Si Nanowire Heterostructures as High-Performance Field-Fffect Transistors. *Nature* **2006**, 441, 489-493.

10 Yi, K. S.; Trivedi, K.; Floresca, H. C.; Yuk, H.; Hu, W.; Kim, M. J. Room-Temperature Quantum Confinement Effects in Transport Properties of Ultrathin Si Nanowire Field-Effect Transistors. *Nano Lett.* **2011**, 11, 5465-5470.

11 Cor Claeys, E. S.; Germanium-Based Technologies from Materials to Devices, 1st ed.; Elsevier: New York, **2007**.

12 Raffy, C.; Furthmuller, J.; Bechstedt, F. Properties of hexagonal polytypes of group-IV elements from first-principles calculations. *Phys. Rev. B* **2002**, 66, 075201-10.

13 Kiefer, F.; Hlukhyy, V.; Karttunen, A. J.; Fassler, T. F.; Gold, C.; Scheidt, E.W.; Scherer, W.; Nylena, J; Haussermann, U. Synthesis, structure, and electronic properties of 4H-germanium. *J. Mater. Chem.* **2010,** 20, 1780-1786

14 Ikonic, Z.; Srivastava, G. P.; Inkson, J. C. Electronic Structure of Twinning Superlattices. *Surf. Sci.* **1994**, *307*,880-884.

15 Picu, R. C.; Borca-Tasciuc, T.; Pavel, M. C. Strain and Size Effects on Heat Transport in Nanostructures. *J. Appl. Phys.* **2003**, *93*, 3535-3539.

16 Bhowmick, S.; Shenoy, V. B. Effect of Strain on the Thermal Conductivity of Solids. J. Chem. Phys. **2006**, *125*, 164513-6.

17 Zhu, L.; Zheng, X. Modification of the Phonon Thermal Conductivity in Spatially Confined Semiconductor Nanofilms Under Stress Fields. *Europhys. Lett.* **2009**, 88, 36003-(5pp).

18 Li, X.; Maute, K.; Dunn, M.; Yang, R. Strain Effects on the Thermal Conductivity of Nanostructures. *Phys. Rev. B* **2010**, *81*, 245318-(11pp).

19 Murphy, K. F.; Piccione, B.; Zanjani, M. B.; Lukes, J. R.; Gianola, D. S. Strain- and Defect-Mediated Thermal Conductivity in Silicon Nanowires. *Nano Lett.*, **2014**, *14*, 3785-3792.

20 Abramson, A. R.; Tien, C.-L.; Majumdar, A. Interface and Strain Effects on the Thermal Conductivity of Heterostructures: A Molecular Dynamics Study. *J. Heat Transfer* **2002**, 124, 963-970.

21 Huang, Y.; Duan, X.; Cui, Y.; Lauhon, L. J.; Kim, K. H.; Lieber, C. M. Logic Gates and Computation from Assembled Nanowire Building Blocks. *Science* **2001,** *294*, 1313-1317.

22 Thelander, C.; Nilsson, H. A.; Jensen; L. E.; Samuelson, L. Nanowire Single-Electron Memory. *Nano Lett.* **2005,** *5*, 635-638.

23 Mathur, N. Beyond the Silicon Roadmap. *Nature* **2002**, *419*, 573-574.

24 Cui, Y.; Wei, Q.; Park, H.; Lieber, C. M. Nanowire Nanosensors for Highly Sensitive and Selective Detection of Biological and Chemical Species, *Science* **2001**, *293*, 1289-1292.

25 Wang, W. U.; Chen, C.; Lin, K. H.; Fang, Y.; Lieber, C. M. Label-Free Detection of Small-Molecule–Protein Interactions by Using Nanowire Nanosensors. *Proc. Natl Acad. Sci. USA.* **2005**,*102*, 3208-3212.

26 Huang, M. H.; Mao, S.; Feick, H.; Yan, H.; Wu, Y.; Kind, H.; Weber, E.; Russo, R.; Yang, P. Room-Temperature Ultraviolet Nanowire Nanolasers. *Science* **2001**, 292, 1897-1899.

27 Barrelet, C. J.; Greytak, A. B.; Lieber, C. M. Nanowire Photonic Circuit Elements. *Nano Lett.* **2004**, *4*, 1981-1985.

28 Kayes, B. M.; Atwater, H. A.; Lewis, N. S. Comparison of the Device Physics Principles of Planar and Radial p-n Junction Nanorod Solar Cells. *J. Appl. Phys.* **2005**, *97*, 114302-(11pp).

29 Hochbaum, **A.** I.; Chen, R. K.; Delgado, R. D.; Liang, W. J.; Garnett, E. C.; Najarian, M.; Majumdar, A.; Yang, P. D. Enhanced Thermoelectric Performance of Rough Silicon Nanowires. *Nature* **2008**, 451, 163-168.

30 Lugstein, A; Mijí´c, M.; Burchhart, T.; Zeiner, C.; Langegger, R.; Schneider, M.; Schmid, U.; Bertagnolli, E. In Situ Monitoring of Joule Heating Effects in Germanium Nanowires by μ-Raman Spectroscopy. *Nanotechnology* **2013**, *24*, 065701-(5pp).

31 Schmotz, M.; Bookjans, P.; Scheer, E.; Leiderer, P. Optical temperature measurements on thin freestanding silicon membranes. *Rev. Sci. Instrum.* **2010**, 81, 114903-3.

32 Tsu , R. and Hernandez, J. G. Temperature dependence of silicon Raman lines. *Appl. Phys. Lett* **1982**, 41, 1016-2018.

33 Périchon, S.; Lysenko, V. ; Remaki, B.; Barbier, D.; Champagnon B. Measurement of porous silicon thermal conductivity by micro-Raman scattering. *J. Appl. Phys.* **1999,** 86, 4700-4702.

34 Pe´richon, S.; Lysenko, V.; Roussel, P.; Remaki, B.; Champagnon, B.; Barbier, D.; Pinard, P. Technology and micro-Raman characterization of thick meso-porous silicon layers for thermal effect microsystems. *Sensors and Actuators* **2000,** 85. 335–339.

35 Liu, X; Wu, X.; Ren, T. In situ and noncontact measurement of silicon membrane thermal conductivity. *Appl. Phys. Lett* **2011**, 98, 174104-3.

36 Huan, S.; Ruan. X.; Zou; J.; Fu, X.; Yang, H. Thermal conductivity measurement of submicrometer-scale silicon dioxide films by an extended micro-Raman method. *Microsyst Technol* **2009**, 15, 837–842.

37 Ángel, E. C; Reparaz, J. S. ; Bresco, J. G.; Wagner, M. R.; Cuffe, J.; Graczykowski, B.; Shchepetov, A.; Jiang, H.; Prunnila, M.; Ahopelto, J.; Alzina, F.; Torres, C. M.S. Reduction of the thermal conductivity in free-standing silicon nano-membranes investigated by non-invasive Raman thermometry. *APL Mater.* **2014**, 2, 012113-6.

38 Balandin, A. A.; Ghosh, S.; Bao, W.; Calizo, I.; Teweldebrhan, D.; Miao, F; Lau, C. N. Superior thermal conductivity of single-layer graphene. *Nano Lett.* **2008**, 8, 902-907.

39 Reparaz, J. S.; Angel, E. C.; Wagner, M. R.; Graczykowski, B.; Bresco, J. G.; Alzina, F.; Torres, C. M. S. A novel contactless technique for thermal field mapping and thermal conductivity determination: Two-Laser Raman Thermometry. *Rev. Sci. Instrum.* **2014**,85, 034901-5.

40 Jalilian, R.; Sumanasekera, G. U.; Chandrasekharan, H.; Sunkara, M. K. Phonon Confinement and Laser Heating Effects in Germanium Nanowires. *Phys. Rev. B* **2006**, *74*, 155421-(6pp).

41 Duzynska, A.; Judek, J.; Zdrojek, M. Temperature-Dependent Nonlinear Phonon Behavior in High-Density Carbon Nanotube Thin Films. *Appl. Phys. Lett.* **2014**, *105***,** 213105-(5pp).

42 Taube, A; Judek, J.; Jastrzębski, C.; Duzynska, A.; Świtkowski, K.; Zdrojek, M. Temperature-Dependent Nonlinear Phonon Shifts in a Supported MoS_2 Monolayer. *ACS Appl. Mater. Interfaces* **2014**, 6, 8959-8963.

43 Gupta, R.; Xiong, Q.; Adu, C. K.; Kim, U. J.; Eklund, P. C. Laser-Induced Fano Resonance Scattering in Silicon Nanowires. *Nano Letters*, **2003**, 3, 627-631.

44 Ghoshal, T.; Maity, T.; Godsell, J. F.; Roy, S.; Morris, M. A. Large Scale Monodisperse Hexagonal Arrays of Superparamagnetic Iron Oxides Nanodots: A Facile Block Copolymer Inclusion Method. *Advanced Materials*, **2012**, *24*, 2390-2397.

45 Biswas, S.; Doherty, J.; Majumdar, D.; Ghoshal, T.; Rahme, K.; Conroy, M.; Singha, A.; Morris, M. A.; Holmes, J. D. Diameter-Controlled Germanium Nanowires with Lamellar Twinning and Polytypes. *Chem. Mater.* **2015**, *27*, 3408-3416.

46 Davidson , F. M.; Lee , D. C.; Fanfair , D. D.; Korgel, B.A. Lamellar Twinning in Semiconductor Nanowires. *J. Phys. Chem. C*, **2007**, *111*, 2929-2935.

47 Reparaz, J. S.; Peica, N.; Kirste, R.; Goni, A. R.; Wagner, M. R.; Callsen, G.; Alonso, M. I.; Garriga, M.; Marcus, I. C.; Ronda, A.; Berbezier, I.; Maultzsch, J.; Thomsen, C.; Hoffmann, A. Probing local strain and composition in Ge nanowires by means of tip-enhanced Raman scattering. *Nanotechnology* **2013**, 24, 185704 (6pp)

48 Nari, J.; Shadi, A. D.; Lauhon, J. L. Origin of Polytype Formation in VLS-Grown Ge Nanowires through Defect Generation and Nanowire Kinking. *Nano Lett.* **2013**, *13*, 3947-3952.

49 Liu, M. S.; Bursill, L. A.; Prawer, S.; Nugent, K. W.; Tong, Y. Z.; Zhang, G. Y. Temperature Dependence of Raman Scattering in Single Crystal GaN Films. *Appl. Phys. Lett.*, **1999**, *74*, 3125-3127.

50 Burke H. H.; Herman, I. P. Temperature Dependence of Raman Scattering in $Ge_{1-x}Si_x$ Alloys. *Phys. Rev. B.* **1993**, *48*, 15016-15024.

51 Hart, T. R.; Aggarwal, R. L.; Lax, B. Temperature Dependence of Raman Scattering in Silicon. *Phys. Rev. B.* **1970**, *1*, 638-642.

52 Menéndez, J.; Cardona, M. Temperature Dependence of the First-Order Raman Scattering by Phonons in Si, Ge, and a-Sn: Anharmonic Effects. *Phys. Rev. B.* **1984**, *29*, 2051-2059.

53 Debernardi, A.; Baroni, S.; Molinari, E. Anharmonic Phonon Lifetimes in Semiconductors from Density-Functional Perturbation Theory. *Phys. Rev. Lett.* **1995**, *75*, 1819-1822.

54 Zhang G.; Zhang, Y-W. Thermal Conductivity of Silicon Nanowires: From Fundamentals to Phononic Engineering. *Phys. Status Solidi RRL*, **2013**, ***7***, 754-(13pp).

55 Sansoz, F. Surface Faceting Dependence of Thermal Transport in Silicon Nanowires. *Nano Lett.* **2011**, 11, 5378-5382.

56 Sahoo, S.; Gaur, A. P. S.; Ahmadi, M.; Guinel, M. J.F.; Katiyar, R. S. Temperature-dependent Raman studies and thermal conductivity of few-layer MoS_2. *J. Phys. Chem. C* **2013**, 117, 9042−9047.

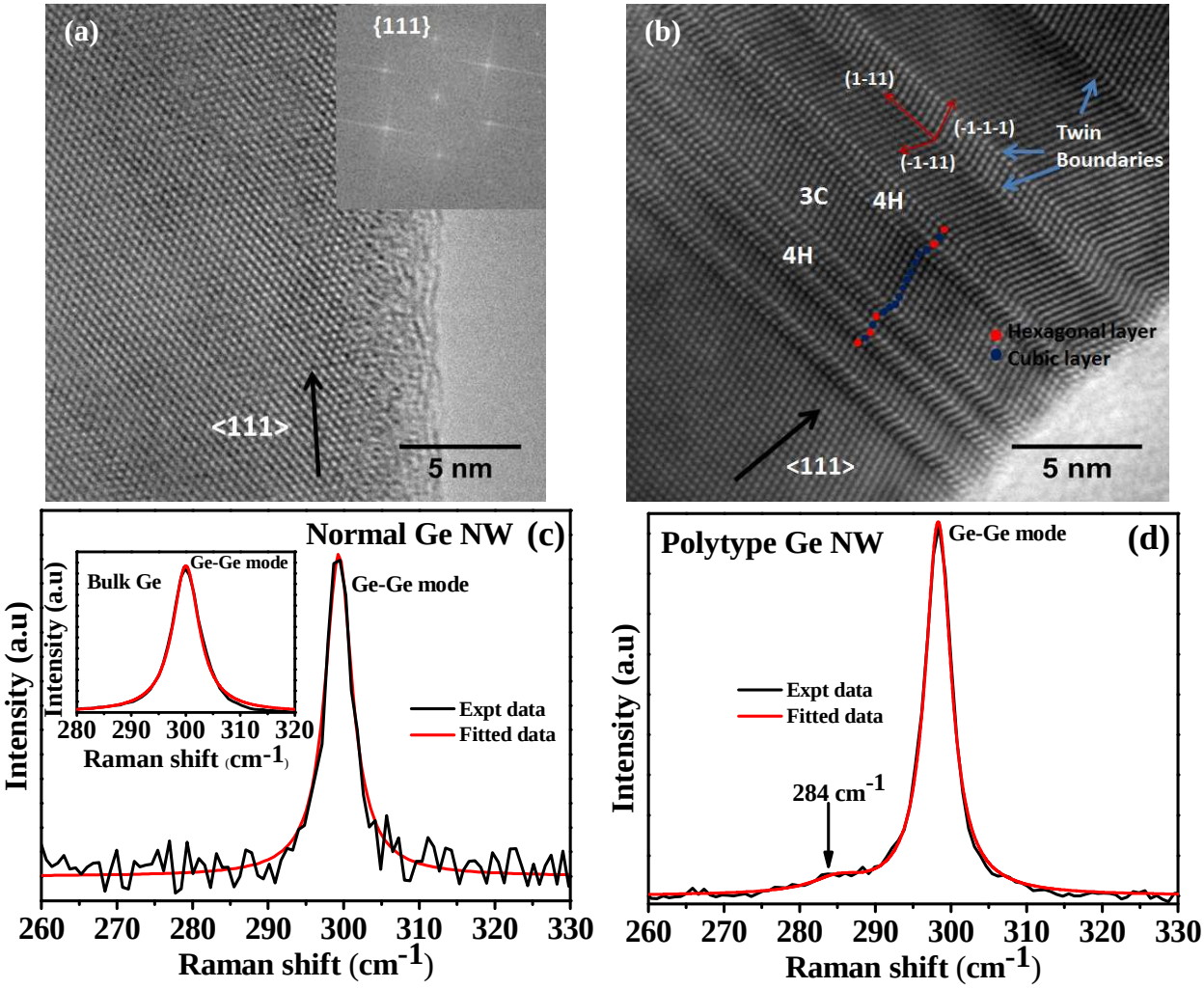

Figure 1: HRTEM images of (a) normal and (b) twinned Ge NWs. Formation of twin boundaries and polytype segments are shown for the twinned NW. The inset of Figure (a) shows the fast Fourier transform pattern (FFT) of normal NW. Part (c) and (d) depicted the Raman spectra of normal and twinned Ge NWs. The Raman spectrum of bulk Ge is displayed in the inset of Figure 1(c).

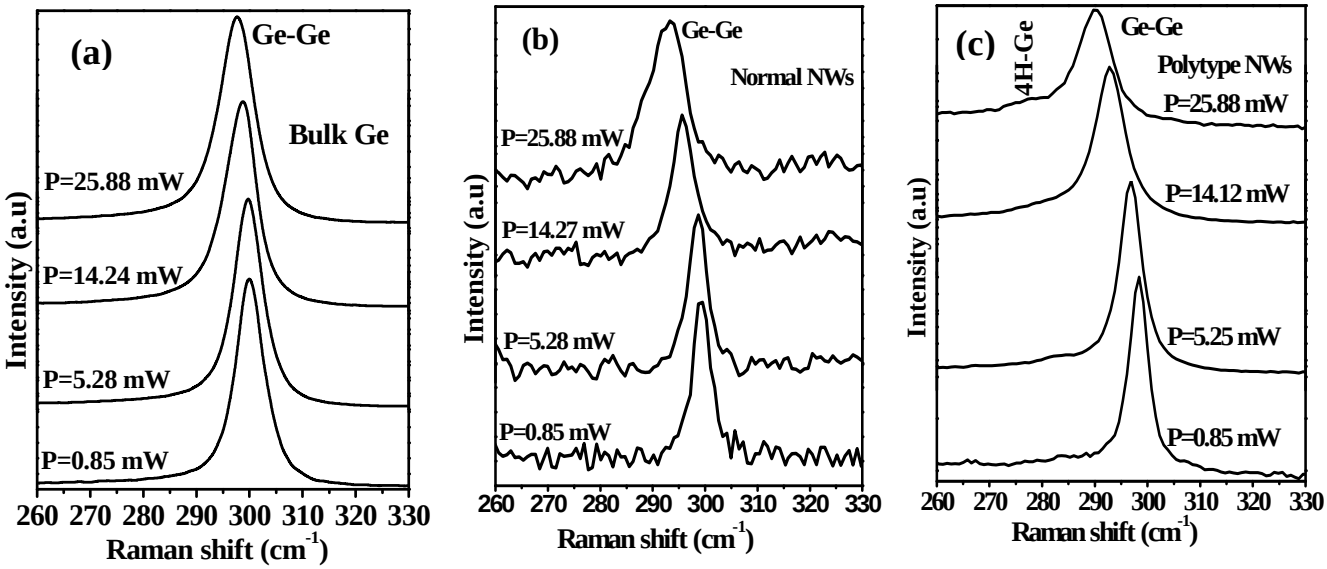

Figure 2: Laser power dependent Raman spectra of (a) bulk Ge, (b) normal NW and (c) twinned NW.

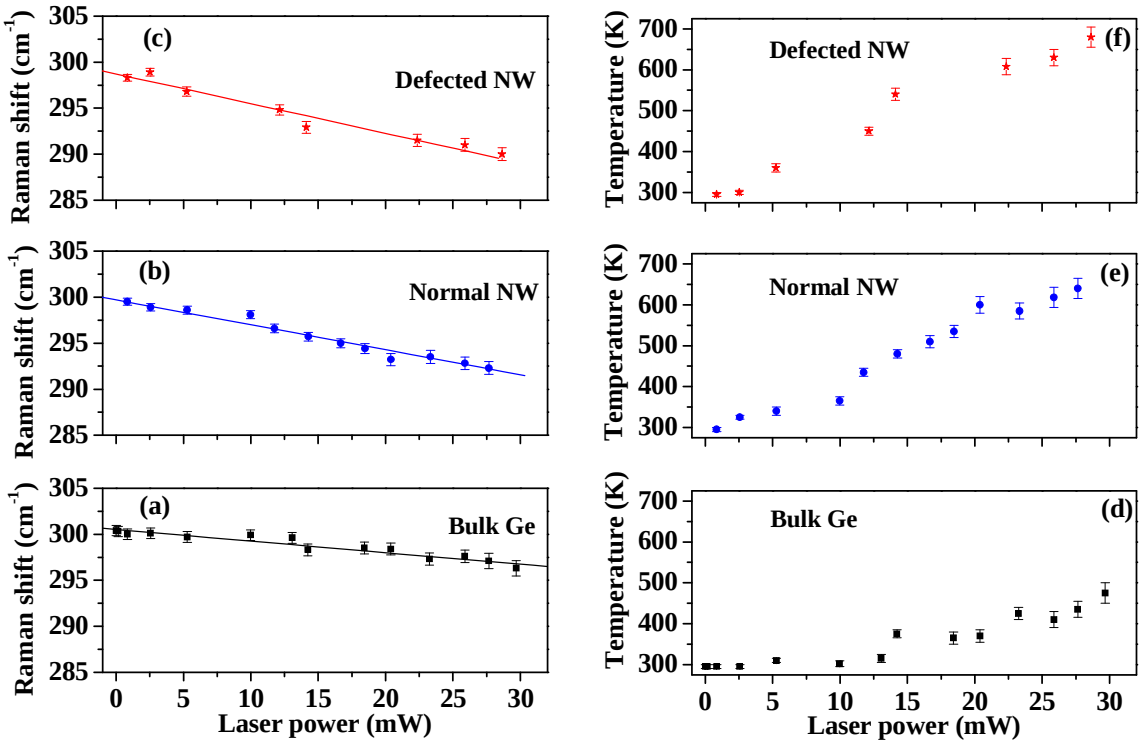

Figure 3. Position of Ge-Ge mode as a function of laser power in (a) bulk Ge, (b) normal Ge NW and (c) twinned Ge NW. Solid lines are linear fit to the experimental data. Local temperature as a function of laser power in (d) bulk Ge, (e) normal Ge NW and (f) twinned Ge NW.

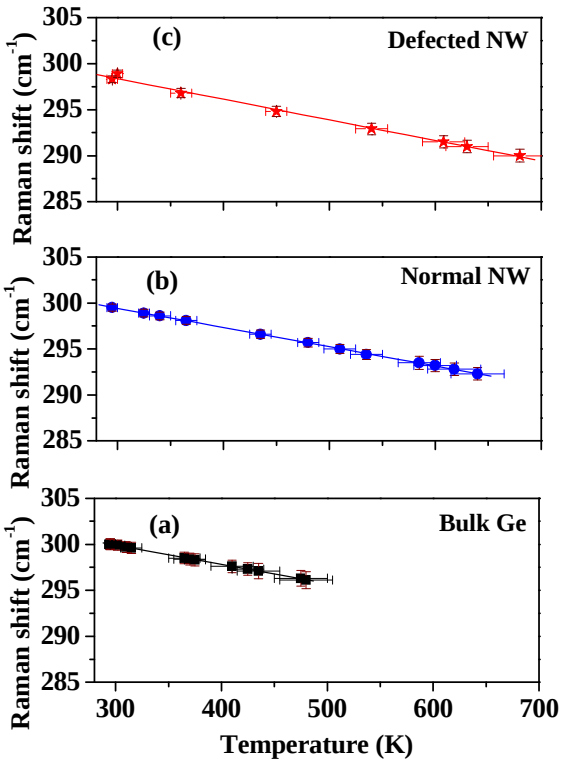

Figure 4. Raman shifts as a function of temperature in (a) bulk Ge, (b) Normal Ge NW and (c) twinned Ge NW. Solid lines are linear fit to the data.

Table of Contents